**Proceedings of the**
**International Conference on Mechanical Engineeringand Renewable Energy 2019**
**(ICMERE2019) 11 – 13 December, 2019, Chittagong, Bangladesh**

**ICMERE2019-PI-177**

# CHARACTERISTIC OF INTERLAYER THICKNESS ON SINGULAR STRESS FIELD IN 3D BONDED JOINT USING FEM

**Md. Jahangir Hossain, and Md. Shahidul Islam**

Dept. of Mechanical Engineering, Khulna University of Engineering & Technology, Khulna-9203, Bangladesh
Jahangirkuetme14@gmail.com, shahidulbitk@gmail.com*

***Abstract***- *Bonded joint is widely used in electronic packaging. In bonded joint two or more materials are joined by adhesive. The joint subjected to mechanical loading developed large stress near the vertex and along the interface edge causing failure of the joint. The interlayer thickness of bonded joint also greatly affects the performance of bonded joint. It is important to determine interlayer thickness for better performance of the joint. In this paper, the characteristic of interlayer thickness of three-layered bonded joint composed of SiC, Resin and SiN is investigated using FEM. The present model can be used to make Integrated Circuit (IC) chip. So far, most of the IC chip is mainly made by bi-material bonded joints. But in the present model are used SiC, Resin and SiN. This model can be operated at higher voltage and carry more currents than bi-material bonded chip. Also this model has the ability to operate at higher temperature and transfer heat at higher rate than bi-material chip. As a result, the complexity of cooing system and cooling cost is greatly reduced. The thickness of interlayer is varied and stress distribution near the vertex and along the interface edge is analyzed using ABAQUS 6.14 software. It is found from the numerical result that the magnitude of stress increases as interlayer thickness increases.*

**Keywords:** Bonded Joint, Stress Singularity, FEM and IC Chip.

## 1. INTRODUCTION

The interlayer thickness is highly responsible for the development of singular stress field near the vertex and along the interface edge for which the joint may fail. So it is necessary to investigate the effect of interlayer thickness on the performance of three-layered bonded joint. In the three-layered bonded joint SiC is used as upper material, Resin as interlayer and SiN as lower material. This model has better electromechanical properties than silicon chip [1].

Benzley developed a finite element method with generalized quadrilateral element having singular point close to corner point [2]. Stephane, Pageau, Sherrill and Biggers developed a method to evaluate order of stress singularity, stress and displacement field around singular point of anisotropic body [3]. Qian and Akisanya analyzed distribution of stress at the corner of interface edge of tri-material joint subjected to uniform variation of temperature [4]. Banks-Sills and Sherer investigated stress intensity factor in case of biomaterial v-notch [5]. Prukvilailert and Koguchi analyzed singular stress field surrounding singular point in 3D dissimilar materials joint [6]. Goglio and Rosstto investigated geometrical effect on the singular stress field close to interface edge of bonded joint [7]. Koguchi and Nakajima investigated the effect of interlayer thickness of three-layered bonded joint on stress singularity [8]. Koguchi and Kimura analyzed singular stress field close to small crack in 3D bonded joint subjected to tensile load [9].

In this research work, the interlayer thickness is varied to analyze its effect on the propagation of singular stress field near the vertex and along the interface edge through Finite Element Method (FEM) using ABAQUS 6.14 software.

## 2. GOVERNING EQUATIONS

The present model consists of isotropic materials. In ABAQUS 6.14 software stress component are determined in Cartesian coordinate. The relation between stress and strain in Cartesian coordinate is given below [10]:

$$\begin{Bmatrix} \sigma_{xx} \\ \sigma_{yy} \\ \sigma_{zz} \\ \sigma_{xy} \\ \sigma_{yz} \\ \sigma_{zx} \end{Bmatrix} = \frac{E}{(1+\nu)(1-2\nu)} \begin{bmatrix} 1-\nu & \nu & \nu & 0 & 0 & 0 \\ \nu & 1-\nu & \nu & 0 & 0 & 0 \\ \nu & \nu & 1-\nu & 0 & 0 & 0 \\ 0 & 0 & 0 & \frac{1-2\nu}{2} & 0 & 0 \\ 0 & 0 & 0 & 0 & \frac{1-2\nu}{2} & 0 \\ 0 & 0 & 0 & 0 & 0 & \frac{1-2\nu}{2} \end{bmatrix} \begin{Bmatrix} \varepsilon_{xx} \\ \varepsilon_{yy} \\ \varepsilon_{zz} \\ \varepsilon_{xy} \\ \varepsilon_{yz} \\ \varepsilon_{zx} \end{Bmatrix} \quad (1)$$

The stress components are transformed from Cartesian to Spherical coordinate as below.

© ICMERE2019

The stress tensor in Cartesian coordinate is

$$\sigma = \begin{bmatrix} \sigma_{xx} & \sigma_{xy} & \sigma_{xz} \\ \sigma_{yx} & \sigma_{yy} & \sigma_{yz} \\ \sigma_{zx} & \sigma_{zy} & \sigma_{zz} \end{bmatrix} \quad (2)$$

The stress tensor in spherical coordinate can be represented as

$$\sigma = \begin{bmatrix} \sigma_{rr} & \sigma_{r\theta} & \sigma_{r\phi} \\ \sigma_{\theta r} & \sigma_{\theta\theta} & \sigma_{\theta\phi} \\ \sigma_{\phi r} & \sigma_{\phi\theta} & \sigma_{\phi\phi} \end{bmatrix} \quad (3)$$

The relation between stress tensor in Cartesian and Spherical coordinate is given as

$$\begin{bmatrix} \sigma_{rr} & \sigma_{r\theta} & \sigma_{r\phi} \\ \sigma_{\theta r} & \sigma_{\theta\theta} & \sigma_{\theta\phi} \\ \sigma_{\phi r} & \sigma_{\phi\theta} & \sigma_{\phi\phi} \end{bmatrix} = \begin{bmatrix} \sin\theta\cos\phi & \sin\theta\sin\phi & \cos\theta \\ \cos\theta\cos\phi & \cos\theta\sin\phi & -\sin\theta \\ -\sin\phi & \cos\phi & 0 \end{bmatrix} * \begin{bmatrix} \sigma_{xx} & \sigma_{xy} & \sigma_{xz} \\ \sigma_{yx} & \sigma_{yy} & \sigma_{yz} \\ \sigma_{zx} & \sigma_{zy} & \sigma_{zz} \end{bmatrix} * \begin{bmatrix} \sin\theta\cos\phi & \cos\theta\cos\phi & -\sin\phi \\ \sin\theta\sin\phi & \cos\theta\sin\phi & \cos\phi \\ \cos\theta & -\sin\theta & 0 \end{bmatrix} \quad (4)$$

Finally, the fundamental relation between stress and strain in Spherical coordinate is given below:

$$\begin{Bmatrix} \sigma_{rr} \\ \sigma_{\theta\theta} \\ \sigma_{\phi\phi} \\ \sigma_{r\theta} \\ \sigma_{\theta\phi} \\ \sigma_{\phi r} \end{Bmatrix} = \frac{E}{(1+\nu)(1-2\nu)} \begin{bmatrix} 1-\nu & \nu & \nu & 0 & 0 & 0 \\ \nu & 1-\nu & \nu & 0 & 0 & 0 \\ \nu & \nu & 1-\nu & 0 & 0 & 0 \\ 0 & 0 & 0 & \frac{1-2\nu}{2} & 0 & 0 \\ 0 & 0 & 0 & 0 & \frac{1-2\nu}{2} & 0 \\ 0 & 0 & 0 & 0 & 0 & \frac{1-2\nu}{2} \end{bmatrix} \begin{Bmatrix} \varepsilon_{rr} \\ \varepsilon_{\theta\theta} \\ \varepsilon_{\phi\phi} \\ \varepsilon_{r\theta} \\ \varepsilon_{\theta\phi} \\ \varepsilon_{\phi r} \end{Bmatrix} \quad (5)$$

## 3. Model of analysis

The present model consists of SiC in the upper portion, Resin as interlayer and SiN in the lower portion. Due to symmetry, quarter of the model is analyzed to reduce computational time and cost. The lower surface is kept fixed in space and 1 MPa distributed load is applied on the upper surface. Then interlayer thickness resin is varied from 0.1 to 8mm (0.1, 0.5, 1, 2, 3, 5, 8 mm) to analyze its effect on stress distribution near the vertex and along the interface edge.

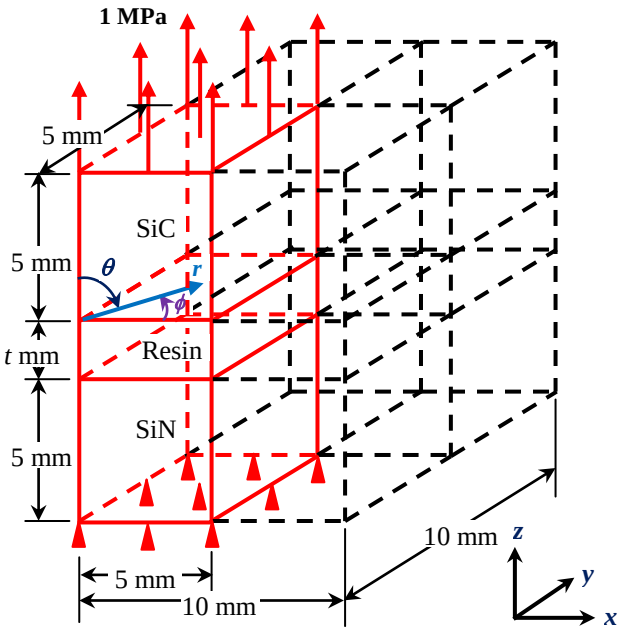


Fig.1: Model for Finite Element Method analysis

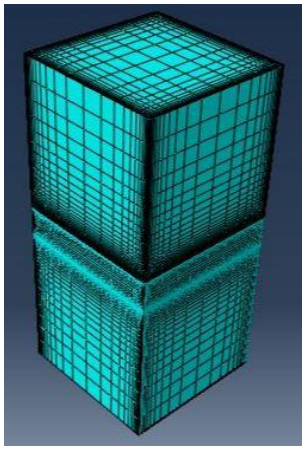

Fig.2: Mesh model

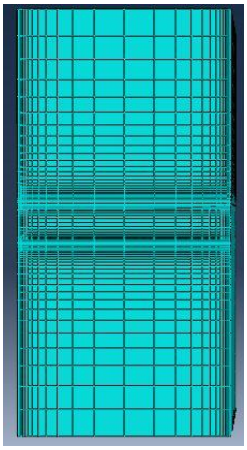

Fig.3: Mesh on *x*-*z* plane

In this analysis, linear hexagonal element is used to generate mesh within model. Fine mesh is used near the vertex and along the interface edge.

Table 1: Property of isotropic materials

| | SiC | Resin | SiN |
|---|---|---|---|
| Young's Modulus, *E* (GPa) | 450 | 2 | 295 |
| Poisson's Ratio, *v* | 0.22 | 0.39 | 0.22 |

## 4. VERIFICATION OF PRESENT ANALYSIS

For interlayer thickness 5 mm, the number of element is varied from 48 thousands to 0.6 million. But stress does not vary when the number of element is 0.5 million or above. Results are taken with approximately 0.5 million elements.

© ICMERE2019

Table 2: Comparison of stress $\sigma_{\theta\theta}$ at $\phi = 36°$ for different element number

| No. of element | Stress $\sigma_{\theta\theta}$ , MPa |
|---|---|
| 48 thousands | 2.0800 |
| 0.3 million | 1.9611 |
| 0.5 million | 1.9433 |
| 0.6 million | 1.9433 |

In this research work, Finite Element method result is compared with a journal paper working on Boundary Element Method for the distribution of normal stress $\sigma_{\theta\theta}$ against dimensionless distance $r/t$ with maximum error of 0.88% [8]. The minimum and maximum element sizes are 0.0001mm and 1mm respectively with 2326581 elements.

Table 3: Comparison of present work and paper work

| Dimensionless distance r/t | Stress in paper work, MPa | Stress in present work, MPa | Error (%) |
|---|---|---|---|
| 0.004 | 1.8900 | 1.8800 | 0.5291 |
| 0.005 | 1.8100 | 1.8005 | 0.5249 |
| 0.030 | 1.2587 | 1.2477 | 0.8739 |
| 0.040 | 1.1900 | 1.1883 | 0.1429 |
| 0.046 | 1.1663 | 1.1600 | 0.5402 |
| 0.051 | 1.1463 | 1.1400 | 0.5496 |
| 0.600 | 0.9600 | 0.9560 | 0.4167 |
| 0.800 | 0.9600 | 0.9569 | 0.3229 |

## 5. RESULT AND DISCUSSION

In the present analysis, the interlayer thickness is varied to analyze its effect on the propagation of singular stress field near the vertex and along the interface edge using ABAQUS 6.14 software and the result are presented a follow.

### 5.1 Maps of stress for *t* = 8 mm

Figures 4 to 9 represent the distribution of stress $\sigma_{ij}$ against radial distance $r$ and angle $\phi$ at both interfaces. The figures show that large stress develops near the vertex and along the interface edge than other regions. So there is high probability of the joint to fail near the vertex and along the interface edge.

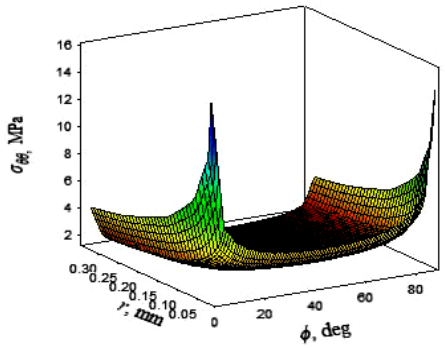


Fig.4: Distribution of stress $\sigma_{\theta\theta}$ against radial distance $r$ and angle $\phi$ at SiC-Resin interface

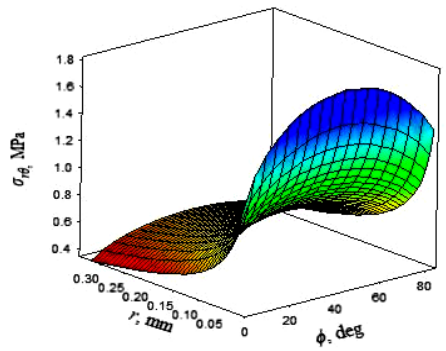


Fig.5: Distribution of stress $\sigma_{r\theta}$ against radial distance $r$ and angle $\phi$ at SiC-Resin interface

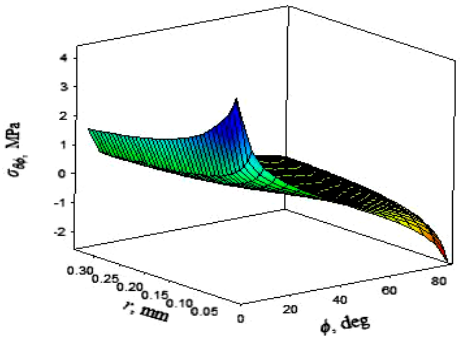


Fig. 6: Distribution of stress $\sigma_{\theta\phi}$ against radial distance $r$ and angle $\phi$ at SiC-Resin interface

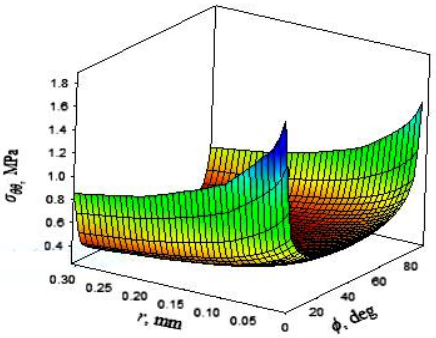


Fig. 7: Distribution of stress $\sigma_{\theta\theta}$ against radial distance $r$ and angle $\phi$ at Resin-SiN interface

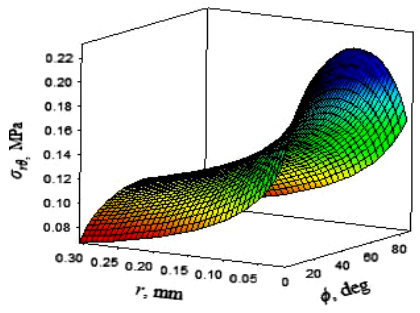


Fig. 8: Distribution of stress $\sigma_{r\theta}$ against radial distance $r$ and angle $\phi$ at Resin-SiN interface

© ICMERE2019

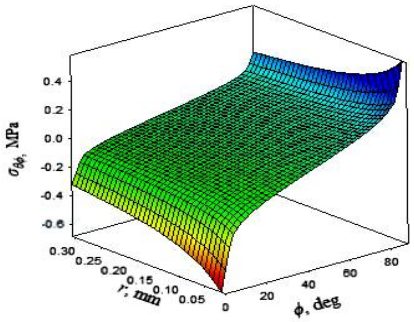


Fig.9: Distribution of stress $\sigma_{\theta\phi}$ against radial distance $r$ and angle $\phi$ at Resin-SiN interface

### 5.2 Variation of stress $\sigma_{ij}$ against radial distance $r$ for various interlayer thicknesses

Figures 10 to 15 show the distribution of stress $\sigma_{ij}$ against radial distance $r$ for various interlayer thicknesses. It is clear from the figures that stress increases with the increase in interlayer thickness and so probability of failure increases.

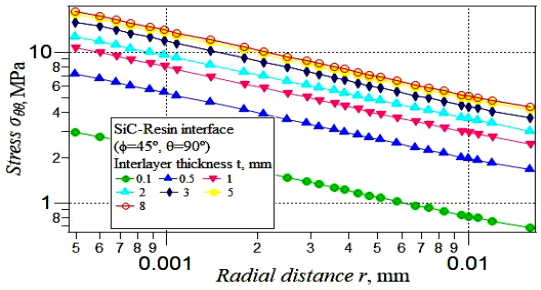


Fig. 10: Distribution of stress $\sigma_{\theta\theta}$ against radial distance $r$ for various interlayer thicknesses at SiC-Resin interface

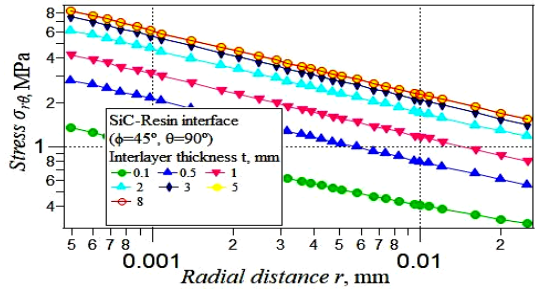


Fig. 11: Distribution of stress $\sigma_{r\theta}$ against radial distance $r$ for various interlayer thicknesses SiC-Resin interface

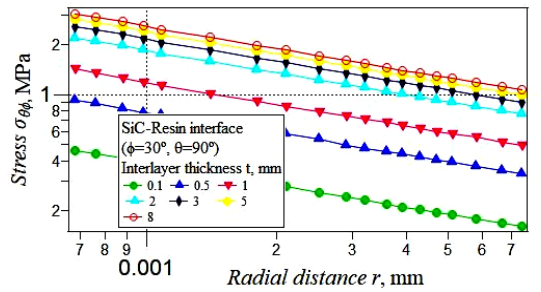


Fig. 12: Distribution of stress $\sigma_{\theta\phi}$ against radial distance $r$ for various interlayer thickness SiC-Resin interface

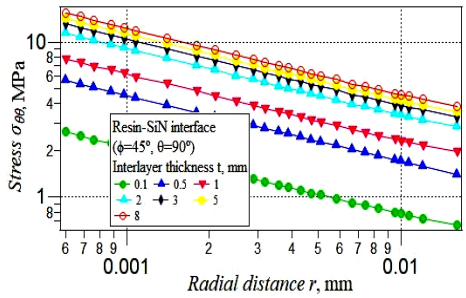


Fig. 13: Distribution of stress $\sigma_{\theta\theta}$ against radial distance $r$ for various interlayer thicknesses at Resin-SiN interface

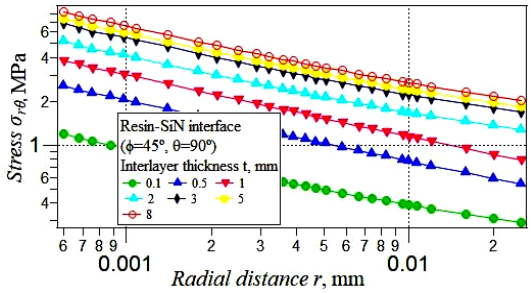


Fig. 14: Distribution of stress $\sigma_{r\theta}$ against radial distance $r$ for various interlayer thicknesses Resin-SiN interface

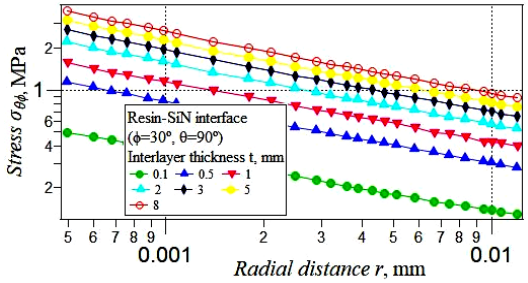


Fig. 15: Distribution of stress $\sigma_{\theta\phi}$ against radial distance $r$ for various interlayer thicknesses Resin-SiN interface

### 5.3 Variation of stress $\sigma_{ij}$ against angle $\theta$ for various interlayer thicknesses

Figures 16 to 21 illustrate the distribution of stress $\sigma_{ij}$ against angle $\theta$ for various interlayer thicknesses. The figures notice that large stress develops at thick interlayer which has high probability to delaminate.

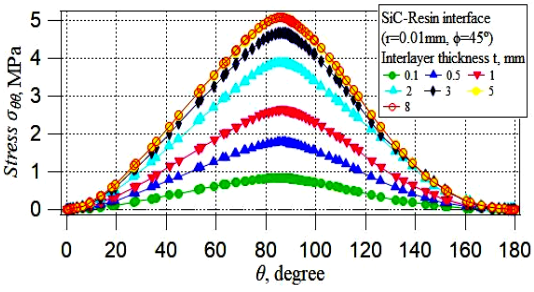


Fig. 16: Distribution of stress $\sigma_{\theta\theta}$ against angle $\theta$ for various interlayer thicknesses at SiC-Resin interface

© ICMERE2019

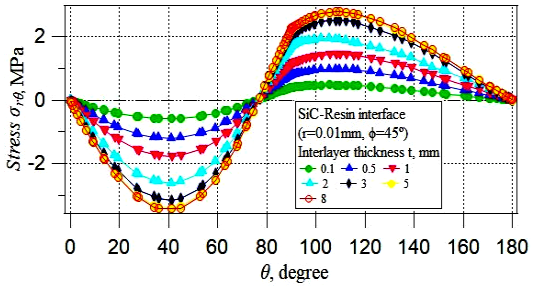


Fig. 17: Distribution of stress $\sigma_{r\theta}$ against angle $\theta$ for various interlayer thicknesses at SiC-Resin interface

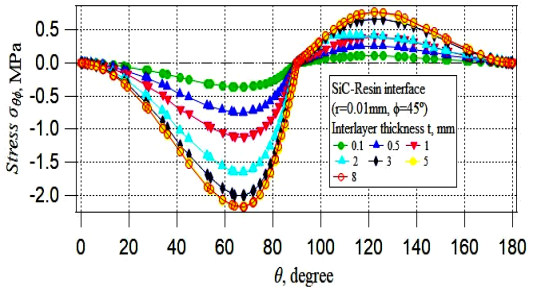


Fig. 18: Distribution of stress $\sigma_{\theta\phi}$ against angle $\theta$ for various interlayer thicknesses at SiC-Resin interface

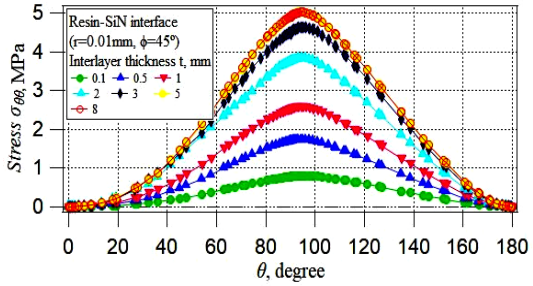


Fig. 19: Distribution of stress $\sigma_{\theta\theta}$ against angle $\theta$ for various interlayer thicknesses at Resin-SiN interface

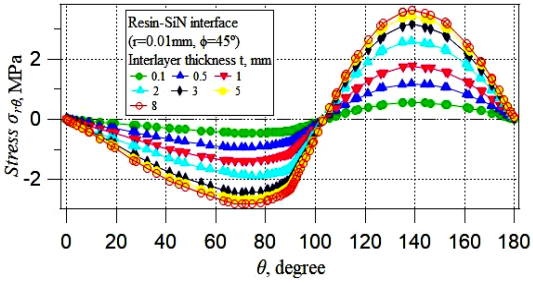


Fig. 20: Distribution of stress $\sigma_{r\theta}$ against angle $\theta$ for various interlayer thicknesses at Resin-SiN interface

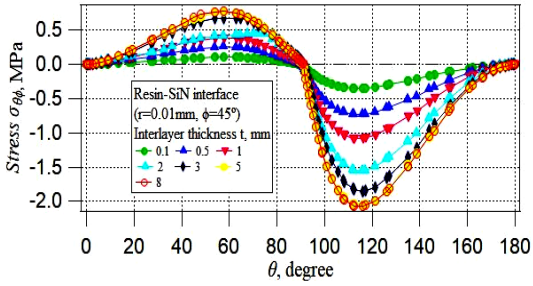


Fig. 21: Distribution of stress $\sigma_{\theta\phi}$ against angle $\theta$ for various interlayer thicknesses at SiC-Resin interface

### 5.4 Variation of stress $\sigma_{ij}$ against angle $\phi$ for various interlayer thicknesses

Figures 22 to 27 represent the distribution of stress $\sigma_{ij}$ against angle $\phi$ for various interlayer thicknesses. The figures show that the stress developed at thick interlayer is larger than that in thin interlayer. So a thick interlayer has higher probability to fail than a thin interlayer.

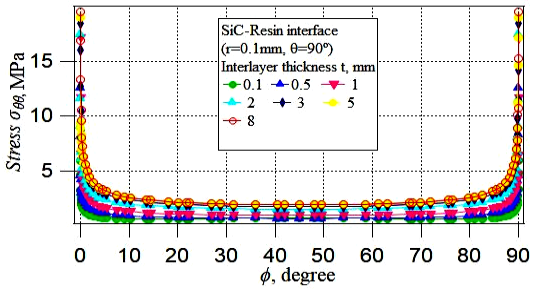


Fig. 22: Distribution of stress $\sigma_{\theta\theta}$ against angle $\phi$ for various interlayer thicknesses at SiC-Resin interface

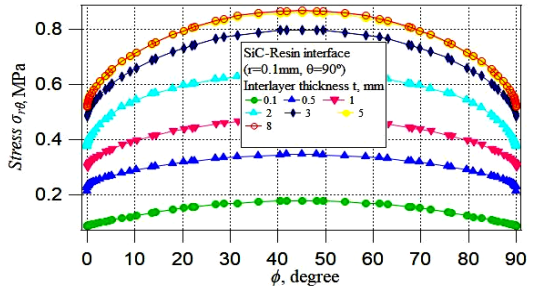


Fig. 23: Distribution of stress $\sigma_{r\theta}$ against angle $\phi$ for various interlayer thicknesses at SiC-Resin interface

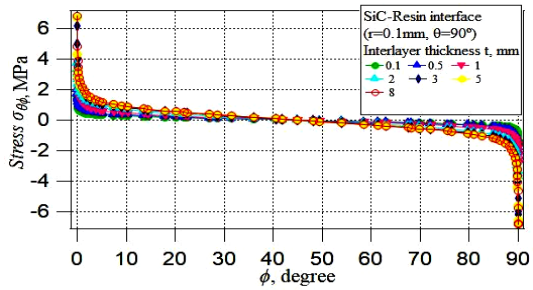


Fig. 24: Distribution of stress $\sigma_{\theta\phi}$ against angle $\phi$ for various interlayer thicknesses at SiC-Resin interface

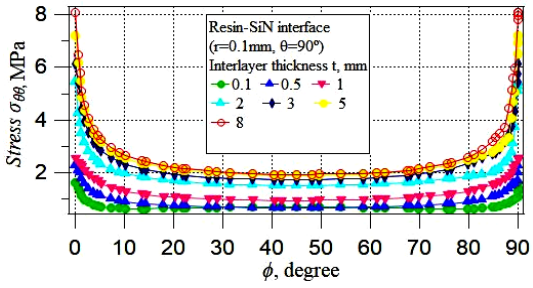


Fig. 25: Distribution of stress $\sigma_{\theta\theta}$ against angle $\phi$ for various interlayer thicknesses at Resin-SiN interface

© ICMERE2019

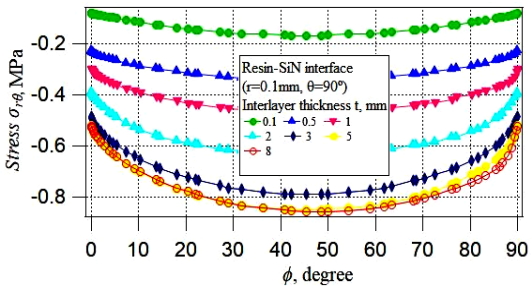


Fig. 26: Distribution of stress $\sigma_{r\theta}$ against angle $\phi$ for various interlayer thicknesses at Resin-SiN interface

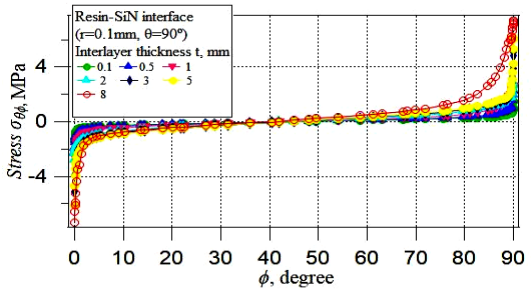


Fig. 27: Distribution of stress $\sigma_{\theta\phi}$ against angle $\phi$ for various interlayer thicknesses at Resin-SiN interface

## 6. Conclusion

The lower surface of the model was kept fixed and 1 MPa tensile load is applied on the upper surface. Then the stress distribution near the vertex and along the interface edge was analyzed. Finally the interlayer thickness was varied to analyze its effect on stress distribution. The following conclusions can be made based on the numerical results of the analysis:

(i) Maximum stress develops near the vertex and along the interface edge for which the joint may debond.

(ii) Large stress development near the vertex and along the interface edge can be prevented by rounding or filleting shape.

(iii) Interlayer thickness should be as thinner as possible, because large stress develops at thick interlayer.

## 7. REFERENCES


[1] Elasser, and T. P. Chow, "Silicon Carbide Benefits and Advantages for Power Electronics Circuits and Systems", *IEEE*, Vol. 90, pp. 969-986, 2002.

[2] S. E. Benzley, "Representation of Singularities with Isoparametric Finite Elements", *International Journal for Numerical Methods in Engineering*, Vol. 8, pp. 537-545.1974.

[3] S. Stephane, Pageau, B. Sherrill, and JR. Biggers, "Finite Element Evaluation of Free-Edge Singular Stress Fields in Anisotropic Materials", *International Journal for Numerical Methods in Engineering*, Vol. 38, pp. 2225-2239. 1995.

[4] Z. Q. Qian, and A. R. Akisanya, "Stress Distribution at the Interface Corner of a Tri-Material Structure", *Journal of Engineering Mechanics*, Vol. 127, pp. 747-753. 2001.

[5] L. Banks-Sills, and A. Sherer, "A Conservative Integral for Determining Stress Intensity Factor of Bimaterial Noych", *International Journal of Fracture*, Vol. 115, pp. 1-26, 2001.

[6] M. Prukvilailert, and H. Koguchi, "Stress Singularity Analysis around the Singular Point on the Stress Singularity line in Three-Dimensional Joints", *International Journal of Solids and Structure*, Vol. 42, pp. 3059-3074, 2005.

[7] L. Goglio, and M. Rosstto, "Stress Intensity Factor in Bonded Joints: Influence of the Geometry", *International Journal of adhesion and Adhesives*, Vol. 30, pp. 313-321. 2010.

[8] H. Koguchi, and M. Nakajima, " Influence of Interlayer Thickness on the Intensity of Singular Stress Field in 3D Three-Layered Joints under an External Load", *Journal of Solid Mechanics and Materials Engineering*, Vol. 4, pp. 1027-1039. 2010.

[9] H. Koguchi, and N. Kimura, " Stress Analysis near a Small Crack within Singular Stress Field in a Three-Dimensional Bonded Joint under a Tensile Load", *Transaction of the JSME*, Vol. 80, No.816, 2014.

[10] D. L. Logan, "A first course in the finite element method", *Cengage learning*, 4th Ed, Appendix C, pp. 748, 2009.


## 8. NOMENCLATURE

| Symbol | Meaning | Unit |
|---|---|---|
| $u$ | Displacement, mm | (mm) |
| $\varepsilon$ | Strain | (mm/mm) |
| $\sigma$ | Stress | (MPa) |
| $E$ | Young modulus | (MPa) |
| $\nu$ | Poisson ratio | Dimentio-nless |
| $\theta$ | Angle | (Degree) |
| $\phi$ | Angle | (Degree) |
| $r$ | Distance from origin | (mm) |
| $t$ | Interlayer thickness | (mm) |

© ICMERE2019